Lyotropic Mesophases of a Fluorinated Surfactant with a Short Nonionic Polar Head in Water

Marie-Hélène Ropers, Marie-José Stébé,* and Véronique Schmitt

Laboratoire de Physico-Chimie des Colloïdes, UMR 7565 CNRS/Université Henri Poincaré Nancy I, Faculté des Sciences BP239, 54506 Vandœuvre-lès-Nancy Cedex, France

Received: December 7, 1998; In Final Form: February 22, 1999

The phase behavior of a water−nonionic fluorinated surfactant $C_6F_{13}C_2H_4SC_2H_4(OC_2H_4)_2OH$ system is reported here. Beyond a reverse micellar phase, three other mesophases are found: a lamellar phase L_α, a bicontinuous cubic domain V_2, and a sponge phase L_3. Its phase diagram is compared with hydrogenated ones. The characterization of these phases and the determination of their structural parameters are performed by SAXS experiments. The cubic phase domain is divided into two cubic phases corresponding to the *Ia*3*d* and *Pn*3*m* structures. They both are described according to ICR and IPMS models. The study of the structural parameters shows that the area per polar group stays constant and the hydrophobic surfactant part is unchanged in all the liquid crystal domains. Epitaxial relationships between the phases are discussed.

1. Introduction

The hydrophobic surfactants are almost insoluble in water and cannot assemble in direct micellar phases. But at high surfactant content, a lot of organized systems are formed as, for example, reverse micelles and liquid crystals as the lamellar (L_α and L_β) and the cubic phases. The lipid-containing systems, with a long alkyl chain or biological amphiphiles, lead to the formation of such structures.[1] In the sixties, Luzzati and coworkers studied those systems and particularly the cubic phase.[2] They put into evidence the so-called bicontinuous cubic phases whose description is today well-known.[1,3] More recently, the same structure has also been found for hydrogenated surfactants with a small polar headgroup as $C_{12}H_{25}(OC_2H_4)_2OH$ (noted $C_{12}EO_2$) in water.[4] In this paper, we contribute to this study by putting in evidence a homologous series of aggregates with a surfactant constituted of a short fluorocarbon chain and two oxyethylene units. Today, the interest focuses again on the cubic phases. A lot of studies reported in the literature concern the mechanism of their formation with temperature and composition, related to the neighboring phases as the lamellar or hexagonal phases.[5]

The properties of the cubic phase (highly viscous, optically isotropic, appearance as glass) are interesting for several applications: proteins crystallization,[6] electrochemical biosensors,[7] or encapsulation of drugs.[8]

Previous investigations on fluorinated surfactants showed their peculiar chemical physical properties. They permit us to decrease strongly the surface tension of water (until 5−6 mN/m) and exhibit a high hydrophobic character.[9] For example, a fluorocarbon chain with 6 carbon atoms is equivalent to a hydrogenated chain with 11 carbon atoms.[10] It has also been shown that their high hydrophobic character could be related to the difference of the cavity volumes formed by the groups CF_3, CH_2, CH_3, and CF_3 in water.[11] Considering those equivalencies, one can make some analogies between hydrogenated and fluorinated surfactants. However, the bilayer formation is more favored in the case of fluorinated compounds than in the case of the hydrogenated ones because of the higher size of the CF_2 group. At the electronic and nuclear level, the presence of the fluorine atoms in the molecule brings a favorable contrast in X-ray and neutron scattering.

In this paper, we investigate the hydrophobic $C_6F_{13}C_2H_4SC_2H_4(OC_2H_4)_2OH$−water system. Its phase behavior is compared to its hydrogenated equivalent. The structural study of the lamellar and cubic phases performed by small-angle x-ray scattering (SAXS) permits us to examine the evolution of the structure with composition and temperature.

2. Experimental Section

Materials. The fluorinated surfactant is $C_6F_{13}C_2H_4SC_2H_4(OC_2H_4)_2OH$ and referred to as $R_6^F\Sigma EO_2$ where Σ stands for $C_2H_4SC_2H_4$. It has been synthesized according to a method derived by Cambon.[12] The Σ moiety has been introduced in order to make the chemical synthesis of the monodisperse amphiphile easier.

Phase Diagram Determination. The phases equilibrium has been determined using the classical methods. The samples were prepared by weighing the required amounts of surfactant and water in well-closed glass vials to avoid evaporation. They were left at controlled temperature for some hours to several days in order to reach equilibrium. The phase diagram has been established between 0 and 60 °C in the whole water−surfactant composition range. The nature of the anisotropic domains were identified by their texture observed with a polarizing microscope. The exact limits of these domains were found out by turbidimetric observations and X-ray diffraction that was also used for the characterization of the liquid crystals.

Small-Angle X-ray Scattering (SAXS). The SAXS experiments concerning the lamellar phase were performed at our laboratory using a camera coupled to a one-dimensional detector (gas ionization from INEL). The X-ray beam is focused by mean of a curved gold/silica mirror. The whole setting is placed in a vacuum caisson to avoid absorption by air. The incident beam wavelength λ is 1.54 Å, and the sample to detector distance is

* To whom correspondence should be addressed. E-mail: stebe@lesoc.u-nancy.fr.

10.1021/jp984662a CCC: $18.00
Published on Web 04/09/1999

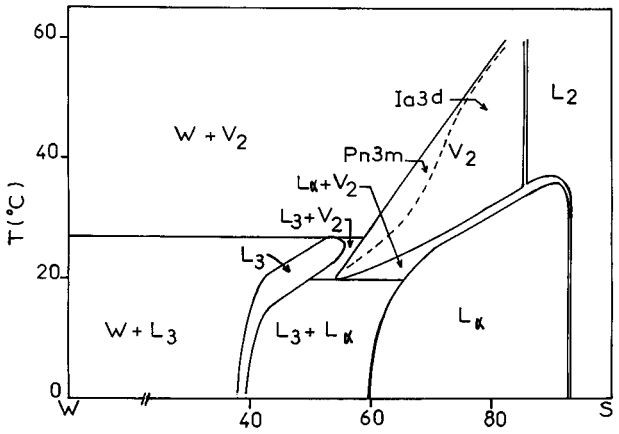

Figure 1. Binary phase diagram of the $C_6F_{13}C_2H_4SC_2H_4(OC_2H_4)_2OH$−water system. L_2 is a reverse micellar phase, L_α the lamellar phase, and L_3 the sponge phase. The reverse cubic domain V_2 is divided into two subregions corresponding to two space groups *Pn*3*m* and *Ia*3*d*.

500 mm. Hence the explored q range is 0.09−0.2 Å^{-1}. The systematic and full characterization of the cubic phases has been obtained with the D43 spectrometer at LURE in Orsay (France). The wavelength is 1.446 Å. An X-ray sensitive plate was used in order to record the two-dimensional scattering patterns, the exposure time was about 10 min. A phosphor imager enables the conversion into scattering profiles $I(q)$. The scattering vector q ranges from 0.03 to 0.4 Å^{-1}.

In all cases, glass capillaries of 0.5 mm diameter were filled with the samples, they were controlled by observation between crossed polarizers before and after the experiment. The temperature is regulated by water circulation in the sample holder. The powder diagram, which facilitates the space group determination, is obtained by rapidly heating the samples (the samples are transferred from a cold bath to the required temperature; the temperature increase is about 15 °C). The spectrum is recorded after the equilibration at the desired temperature for 15 min. The spectra did not change even after 1 h, proving that this treatment did not lead to metastable phases.

3. Phase Diagram

The surfactant studied in the present work is of the "hydrophobic" type, as shown by the phase diagram reported in Figure 1. Dilute surfactant always appears "water insoluble"; mesophases are formed between 38% and 100% in weight of surfactant. At very high surfactant contents, a reverse micellar phase (L_2) exists whatever the temperature. For surfactant amounts between 60% and 92%, a lamellar phase L_α forms that completely melts at 35 °C. This lamellar phase transforms, at high temperature, into a large cubic phase, noted V_2, characterized by its isotropy and very high viscosity. By dilution, the cubic phase generates a sponge phase classically noted L_3. This sponge phase extends from 38% to 60% in weight of surfactant and from 5 to 25 °C. Let us remark that the L_3 phase is very sensitive to the surfactant concentration at low temperature, in view of the narrowness of the domain between 5 and 15 °C. The existence of this domain does not permit the lamellar phase to coexist with water. Except for this feature, this phase diagram resembles the $C_{12}EO_2$ hydrogenated surfactant−water one published by Tiddy.[13] It presents the advantage of a vast cubic region that allows a convenient exploration.

4. Lamellar Phase (L_α)

The lamellar phase extends over a wide domain, showing its stability against temperature (between 10 and 35 °C) and

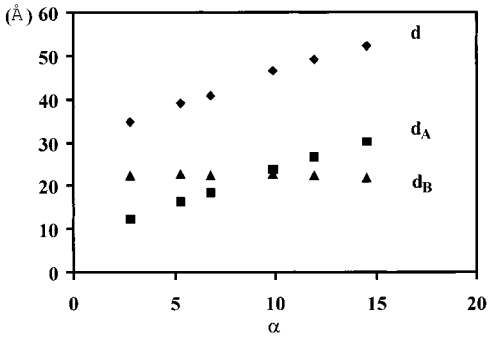

Figure 2. Evolution of the repetition distance d (◆) and the hydrophilic and hydrophobic thickness of the bilayer d_A (■) and d_B (▲) deduced from the SAXS experiments in the lamellar phase as a function of dilution where α is the number of water molecules per surfactant molecule.

TABLE 1: Repetition Distances (*d*) and Surfaces per Polar Head (*S*) of the Samples Studied in the Lamellar Phase

water wt %	9.0	15.6	19.2	25.8	29.5	33.8
α	2.8	5.3	14.5	9.9	11.9	6.8
d (Å) at 10 °C	34.9	39.0	40.7	46.6	49.0	52.1
S (Å^2)	37.8	37.5	38.1	37.3	38.0	38.7

concentration (between 60 and 92% of weight surfactant). Its structure is very well-known; it consists of a periodical stacking of surfactant bilayers separated by water (smectic order). This periodical stacking gives rise to a Bragg first-order reflection at q^*, the periodicity in real space is then directly deduced from the peak position: $d = 2\pi/q^*$. The Bragg distances have systematically been determined in the whole lamellar domain (Table 1). As expected, the bilayer thickness d increases upon addition of water (Figure 2). Moreover, no temperature effect is noticeable (for 91 wt % of surfactant, d decreases from 36 to 35 Å from 5 to 35 °C).

From simple geometrical considerations and knowing the surfactant and water molar volumes V^S and V^W, one can deduce the area per polar head S:

$$S = \frac{2(V^S + \alpha V^W)}{dN_A}$$

where α is the number of water molecules per surfactant molecule and N_A is the Avogadro number. The molar volumes related to the surfactant molecule were obtained previously.[14] The difference between the molar volumes of pure surfactant and in dilute solutions does not exceed 5%. As a consequence V^S corresponds to the molar volume of pure surfactant (V^S = 343.8 cm^3 mol^{-1}). Area per polar group data are given in Table 1. By considering the bilayer hydrophobic part as the fluorocarbon chain C_6F_{13} plus the junction $C_2H_4SC_2H_4$, one can reach the hydrophobic and hydrophilic thickness of the bilayers d_B and d_A and thus the thickness of the hydrophobic chains l_B (V^B = 254.7 cm^{-3} mol^{-1}).[15] The experimental results (Figures 2 and 3) show that the bilayer swelling does not modify either the surfactant area per polar head ($S = 38 \pm 1$ Å^2) or the hydrophobic chain that hence adopts a partially extended conformation: $l_B = 11.2 \pm 0.5$ Å (the extended conformation gives $l_B^{max} = 14.4$ Å). The bilayer hydrophilic part, which corresponds to both the oxyethylene chains and the possible water film, globally increases with water content. In the present case, one can evaluate these two contributions separately by taking advantage of the very attenuated second Bragg reflection (the intensity ratio between the second and the first peak is lower than 2%). This peculiar feature is due to a vanishing form factor

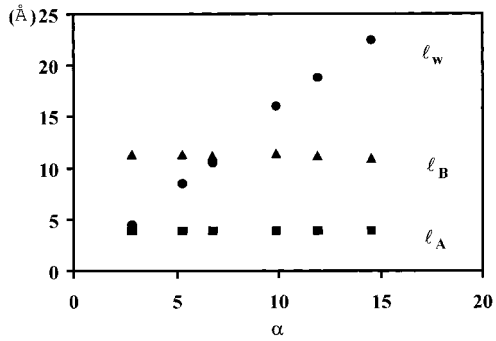

Figure 3. Evolution of the chains and the water film thickness with dilution: (●) l_W water film thickness; (■) l_A thickness of the hydrophilic chain; (▲) l_B thickness of the hydrophobic chain.

of the oriented infinite bilayer at $2q^*$. This same behavior has already been encountered for fluorinated surfactants and for hydrogenated ones where the first-order reflection is not observable.[16,17] The modelization of the diffracted intensity directly gives the oxyethylene chain length l_A and, as a consequence, the water film thickness l_W (Figure 3). In all cases, the only value of l_A that permits us to minimize the intensity ratio between the second and the first peaks is equal to that of the thickness of two oxyethylene groups in a meander conformation (2EO = 3.5 Å).[18] As soon as the lamellar phase forms (at the lower value of α), there is a free water layer $l_W = 5 \pm 1$ Å and the hydrophilic chain is fully folded back since l_A is about 4 Å ($l_A^{min} = 3.9$ Å). As water is incorporated, only the water layer thickness l_W increases: from 5 to 22 Å whereas l_A stays constant and equal to 4 Å. Thus the oxyethylenic chain adopts a given conformation, independent of the composition (meander conformation). The effect of water addition is to increase the water film thickness without modification of the hydration. Consequently, the behavior of the fluorinated surfactant $R_6^F\Sigma EO_2$ in the lamellar phase is different from the one observed in the case of the fluorinated $C_6F_{13}CH_2(OC_2H_4)_n$ ($n = 4, 5, 6$) where the thickness l_A increases regularly with water content.[11,16]

5. Cubic Phase (V_2)

This phase is formed between 15 and 60 °C and at a surfactant concentration ranging from 55 to 85%, corresponding to a number of water molecules per surfactant molecule varying from 4 to 23. It appears isotropic and very viscous. Because the surfactant behavior is largely marked by its hydrophobic character, since it forms reverse micelles, it is likely a reverse cubic phase. This point will be confirmed later on (see below). The SAXS experiments performed throughout the cubic domain, as a function of both concentration and temperature, show the existence of two different cubic structures. Their existence limit is reported in Figure 1 (dotted line). Typical scattering spectra of samples belonging to these two cubic domains are reported in Figure 4a,b (the insets correspond to an expanded intensity scale in order to expose the higher order peaks). The relative positions of the Bragg reflections and their intensities [(1: vvs, $2/\sqrt{3}$; vs, $\sqrt{7/3}$; w, $2\sqrt{2/3}$; w, $\sqrt{10/3}$; m, $\sqrt{11/3}$; s) and (1: vs, $\sqrt{3/2}$; s, $\sqrt{2}$; w, $\sqrt{3}$; m, 2)] are consistent respectively with the body-centered *Ia*3*d* and primitive *Pn*3*m* space groups. The two cubic structures are often encountered in lyotropic systems; they are both of the bicontinuous type.[4,19] In our system, the *Pn*3*m* structure only exists for the higher temperatures. The domain is much smaller than that for the *Ia*3*d* structure. The higher the surfactant concentration, the more stable the *Ia*3*d* structure.

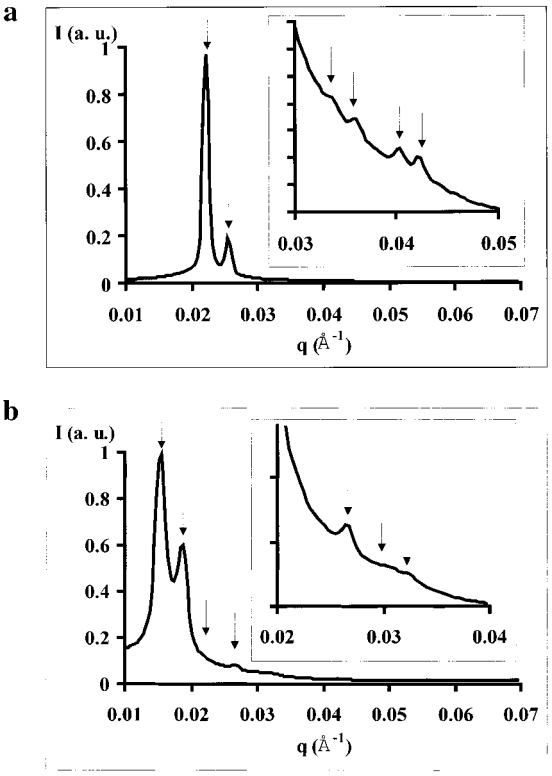

Figure 4. (a) Scattering profile of the sample containing 75% of surfactant at 40 °C belonging to the *Ia*3*d* space group. The same profile is represented in a extended scale as an inset. (b) Scattering profile of a 65% surfactant sample at 30 °C belonging to the *Pn*3*m* space group. The same profile is represented in a extended scale as an inset.

Contrary to what has been observed by Ström[20] and Tiddy,[21] i.e., a refractive index discontinuity between these two groups, we do not observe an interface between the two cubic phases: if the coexisting domain exists, it must be very thin.

The experimental Bragg distances deduced from the SAXS experiments allow the determination of the structural parameters and their evolution with either concentration or temperature. For the *Ia*3*d* space group, the first peak originates from the Bragg reflection of the [211] planes (where 211 are the Miller indices), hence the lattice parameter a_I is calculated by $a_I = d_{211}\sqrt{6}$ from the repetition distance $d_{211} = 2\pi/q^*$, directly deduced from the first peak position q^*. Similarly, the first peak in the *Pn*3*m* space group results from the [110] planes Bragg reflection and hence the lattice parameter a_P is given by $a_P = d_{110}\sqrt{2}$ where the planes distance d_{110} is deduced from the first peak position. These lattice parameters a_I and a_P are reported in Figure 5a,b versus dilution, i.e., versus α, the number of water molecules per surfactant molecule. Tables 2 and 3 give values of a_I and a_P for some compositions chosen regularly in the cubic domain. The temperature does not affect significantly the lattice parameter: between 30 and 60 °C, a_I decreases from 111 to 108 Å for 80 wt % of surfactant. Therefore we assume that a_I and a_P are only concentration dependent. They are of the same order of magnitude as those obtained by Funari for the hydrogenated analogue surfactant $C_{12}EO_2$ in water.[4]

Note that it was impossible to obtain a powder diagram for the cubic samples close to 20 °C. Indeed, the 2D scattering spectra exhibit some Bragg spots and diffuse scattering around them. According to Clerc, the lines joining the Bragg speckles reveal dynamic fluctuation effects that characterize the diffuse scattering.[22] These authors conclude that this phenomenon may come from the collective deformation modes of the labyrinths.

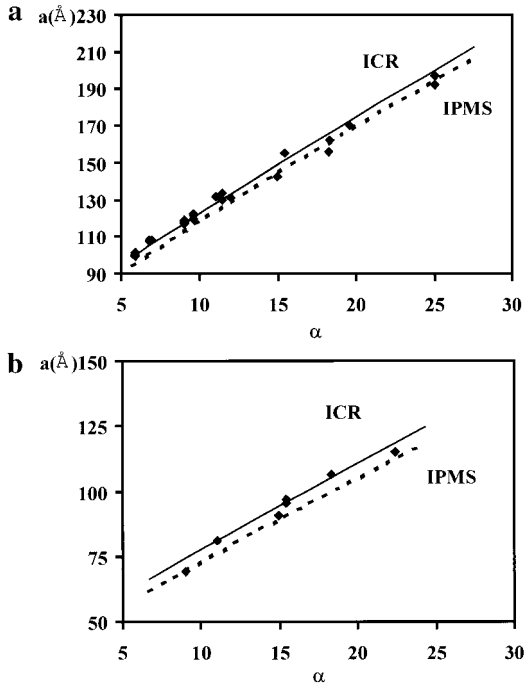

Figure 5. Lattice parameter versus dilution in the space group (a) *Ia*3*d* and (b) *Pn*3*m*: (◆) experimental data; (—) lattice parameter calculated from the ICR model; (- - -) lattice parameter calculated from the IPMS model.

TABLE 2: Geometrical Parameters in the Structure *Ia*3*d*

water wt %	17.2	25.2	29.6	35.1	39.1	40.8	46.8
α	5.9	9.6	12.0	15.4	18.3	19.6	25.0
d (Å)	41.5	49.0	53.6	63.3	66.1	69.5	80.3
a_I (Å)	101.7	120.0	131.3	155.0	162.0	170.2	197.0
L (Å)	35.9	42.4	46.4	54.8	57.2	60.2	69.5
R (Å)	14.5	18.7	21.3	26.4	28.4	30.3	36.4
S (Å^2)	39.3	40.1	40.6	39.0	41.0	40.6	40.7
l_B (Å)	9.5	9.7	9.7	10.2	9.9	9.9	10.1

TABLE 3: Geometrical Parameters in the Structure *Pn*3*m*

water wt %	24.0	27.9	34.4	39.1	44.1
α	9.0	11.0	14.9	18.3	22.4
d (Å)	48.7	57.3	64.3	75.4	81.3
a_P (Å)	68.9	81.0	90.9	106.6	115.0
L (Å)	59.6	70.2	78.8	92.3	99.6
R (Å)	16.6	20.3	24.1	29.4	32.8
S (Å^2)	43.2	40.0	41.5	39.5	41.3
l_B (Å)	10.0	9.7	9.5	10.0	9.7

Furthermore, Imai observes strong fluctuations in intensity in the diffraction pattern of the cubic phases of the $C_{16}EO_4$−water system.[23] According to them it was due to the fluctuations of domains trapped in a metastable state. In our case we observe these two phenomena even over 4 h.

To get further insight about the structural parameters, one can use two descriptions: either the interconnected rod (ICR) model established by Luzzati or the description proposed by Scriven based on the infinite periodic minimal surfaces (IPMS) of Schwarz.[2,24] We exploit our SAXS data using these two descriptions.

(a) ICR Model. The *Ia*3*d* cubic phase can be seen as two interwoven but independent networks of rods connected three by three (Figure 6a). Similarly, the *Pn*3*m* cubic structure consists of two interwoven networks of rods connected four by four (Figure 6b). In these models, all the rods are assumed to have the same length and radius. One can notice the peculiar feature of the enantiomeric nature of the two networks for the *Ia*3*d* structure.[25] In our case of reverse cubic phases, the rods are filled with the hydrophilic headgroups and the water. The surface of the cylinders corresponds to the hydrophilic−hydrophobic surfactant interface. From simple geometrical considerations, Luzzati and co-workers have derived the structural parameters for the *Ia*3*d* cubic phase.[3] The same procedure used for the *Pn*3*m* structure leads to analogous relations.[26] The rod length *L* is related to the lattice parameter by $L = a_I/\sqrt{8}$ for *Ia*3*d* and by $L = a_P\sqrt{3}/2$ for the *Pn*3*m* structure. The hydrophilic volume fraction (surfactant polar head plus water) can be written as

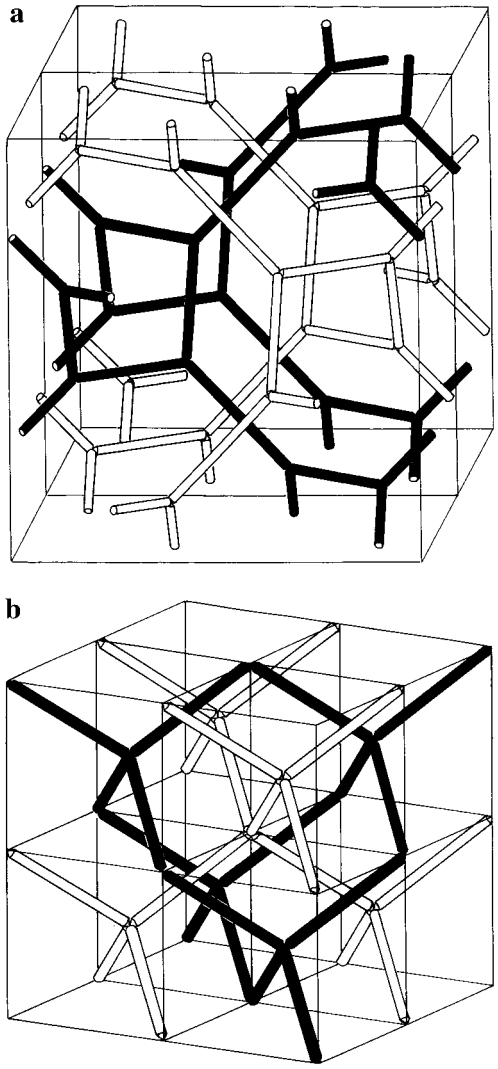

Figure 6. Schematic representation of the cubic phases using the ICR model: (a) *Ia*3*d* structure where two unit cells are drawn in order to show the enantiomeric networks; (b) *Pn*3*m* structure with eight tetrahedron unit cells.

$$\Phi_V^A = \frac{V^A + \alpha V^W}{V^S + \alpha V^W} = \frac{n\pi R^2 L(1 - k_V R/L)}{a^3} \qquad (1)$$

where *n* is the number of rods per cell ($n = 24$ for *Ia*3*d* and $n = 4$ for *Pn*3*m*), *L* is the rod length, *a* is the lattice parameter, and k_V is a constant resulting from the volume calculation of a rod. It takes the value $8/3\sqrt{3\pi}$ for *Ia*3*d* and $2\sqrt{3}/\pi \tan \beta$ where $\beta = 35.25°$ for the *Pn*3*m* structure. V^A is the hydrophilic molar volume ($V^A = 89.1$ cm^3 mol^{-1}). Knowing the composition, the lattice parameter, and hence the rod length *L* of the considered sample, we can deduce the hydrophilic radius from (1). Taking

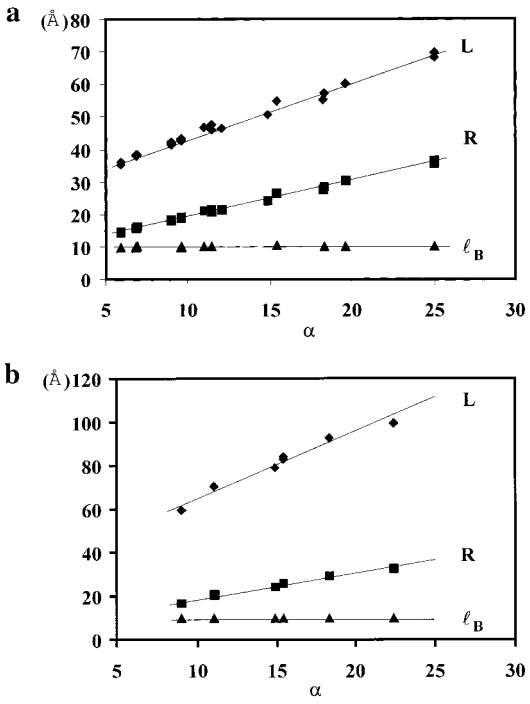

Figure 7. Evolution with dilution of the structural parameters in the (a) *Ia*3*d* and (b) *Pn*3*m* cubic phases using the ICR model. (◆) L is the rod length, (▲) l_B is the thickness of the hydrophobic chains, and (■) R is the rod radius (lines are guides for the eyes).

a volume fraction equal to unity, one can also determine, using (1), the total radius R_t (enclosing both hydrophilic and hydrophobic parts plus water) and deduce the fluorocarbon chains thickness l_B ($l_B = R_t - R$).

The calculation of the rod surface leads to the following expression for the area per polar head:

$$S = \frac{2(V^A + \alpha V^W)(1 - k_S R/L)}{N_A R(1 - k_V R/L)} \tag{2}$$

where $k_S = 4/\sqrt{3}\pi$ for the *Ia*3*d* structure and $3\sqrt{3}/\pi \tan\beta$ with $\beta = 35.25°$ for the *Pn*3*m* structure.

The structural parameters of the cubic phases, calculated using the just exposed ICR model are summarized in Tables 2 and 3 and reported in Figure 7a,b for *Ia*3*d* and *Pn*3*m*, respectively. The surfactant hydrophobic thickness stays constant upon dilution ($l_B = 10 \pm 1$ Å) whatever the structure. If we compare this value with that in an extended chain conformation ($l_B^{max} =$ 14.4 Å), it appears that in the cubic phases, the chains adopt a folded bow conformation. The area per polar head is almost unchanged throughout the cubic domain with a mean value of 40 ± 1 Å^2 whereas both the rod length and hydrophilic radius increase with dilution. The continuous lines represent the theoretical values of R, l_B, and L obtained as follows. From eq 1, for α varying from 5 to 25, the ratio R/L is calculated and, then, by considering a constant area per polar head equal to 40 Å^2, R and L are deduced. The calculated rod dimensions are in good agreement with those deduced from experiments. Note that some authors observe a length of rods L close to twice the radius in the *Ia*3*d* structure.[1] The values of R/L calculated directly from (1) without assumption vary between 0.41 and 0.53, proving that this ratio is not constant but stays nevertheless close to 0.5. Similarly, in the *Pn*3*m* structure, this same ratio evolves between 0.25 and 0.35. It is noteworthy that the radius of the rods is equal for the two structures at the same composition (see Tables 2 and 3). The two structures are then distinguishable only by the lengths and the connections of the rods.

We chose a reverse cubic phase to describe the system. If we assume a direct cubic phase, where the rods are filled with the fluorocarbon chains, the hydrophobic radius and the area per polar head are calculated from the lattice parameter and the appropriate volume fraction through expressions equivalent to (1) and (2). The obtained values are not reasonable, showing that the assumption of direct structures has to be ruled out.

(b) Description in Terms of Periodic Minimal Surfaces (IPMS). In this description, the cubic phase is seen as a continuous bilayer whose midsurface is a Schwarz's periodic minimal surface.[24] For the *Ia*3*d* structure, the minimal surface is a gyroid noted G and for the *Pn*3*m* the Schwarz's D surface. A surface parallel to the minimal surface displaced from it by a distance l has an area A related to the minimal surface one A_0 by[27]

$$A = A_0 + 4\pi\chi l^2 \tag{3}$$

where χ is the Euler characteristic of the surface. The minimal surface area A_0 is related to the lattice parameter a through $A_0 = 2Ca^2$. Both χ and C depend on the surface topology. They are respectively equal to -8 and 3.091 for the gyroid surface and to -2 and 1.919 for the D surface. Here we consider the parallel surface as the interface between the hydrophilic and hydrophobic parts of the surfactant. In the case of reverse cubic phases, the bilayer is made of the fluorocarbon chains; hence the hydrophobic volume fraction can be expressed as

$$\Phi_V^B = \frac{V^B}{V^S + \alpha V^W} = 2C\left(\frac{l_B}{a}\right)\left(1 + \frac{2\pi\chi}{3C}\left(\frac{l_B}{a}\right)^2\right) \tag{4}$$

from which one deduces the hydrophobic chain length l_B by knowing the lattice parameter a. It is constant and equal to 10 ± 1 Å for both the *Ia*3*d* and *Pn*3*m* structures. Again, using a volume fraction equal to 1, one can extract the total length l_t:

$$1 = 2C\left(\frac{l_B}{a}\right)\left(1 + \frac{2\pi\chi}{3C}\left(\frac{l_B}{a}\right)^2\right) \tag{5}$$

and estimate the hydrophilic part (oxyethylene chain length plus water) thickness by $l_A + l_W = l_t - l_B$. Then the area of the parallel surface A can be calculated through (3) with $l = l_B$, and the area per polar head becomes

$$S = \frac{AV^B}{N_A \Phi_V^B a^3} \tag{6}$$

Using this formalism, we deduce $l_B = 10 \pm 1$ Å and $S = 39 \pm 1$ and 40 ± 1 Å for the G and D surfaces, respectively.

(c) Comparison of the Two Models. The values of the surface per polar group S and the hydrophobic thickness l_B obtained from the two models agree very well. On Figure 5a,b, the experimental values of the lattice parameter are reported with the calculated values of the lattice parameter on the basis of two previous descriptions considering the mean value $S =$ 40 Å. The difference between the calculated lattice parameters and the experimental value is always less than 5 Å. This confirms the similarity of the two models in the case of this system and this concentration range. This cubic phase may also be described either by the ICR model or by the IPMS model. Otherwise, it has already been proved in another system (DDAB−water−styrene) that at low water volume fractions the

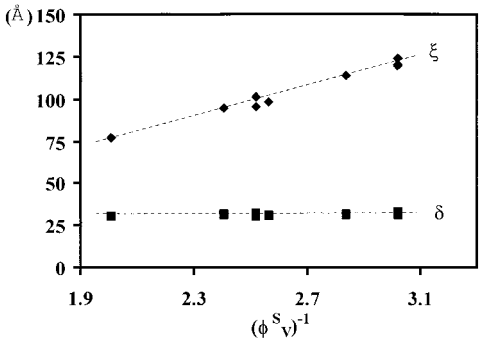

Figure 8. Evolution of the correlation length ξ and the dry bilayer thickness δ versus $(\Phi^S)^{-1}$.

ICR model can apply and at high water fractions the IPMS model is the more convenient.[20] Both models are used today,[4,20] but we must keep in mind that the IPMS model seems to be more realistic. Indeed, this model (where water fills the space between the bilayers) implies a constant hydrophobic tail thickness (for a constant mean curvature at each point), the hydrophilic thickness value depends on the location. If one moves from a node to a place between two nodes, the hydrophilic thickness undergoes small variations. Besides, in the ICR model, it is assumed that the rods have the same radius with a constant hydrophilic thickness and the hydrophobic tails must fill the space between the rods. As the hydrophobic volume around the nodes is higher than that between the nodes, the derived hydrophobic thickness value is a mean value. Although the two models are different, we found the same value for the hydrophobic thickness $l_B = 10 \pm 1$ Å. Nevertheless, it is more conceivable to fill the space between the bilayers by varying the water amount rather than by modifying the hydrophobic chain conformations, leading to a more appropriate description by the IPMS model.

6. Sponge Phase

The sponge phase, first referred to as an "anomalous isotropic phase", is a very fluid isotropic phase (characterized by the exhibition of birefringence upon gentle shaking). Its structure has often been studied, both experimentally and theoretically, in particular by Cates and Porte.[28,29] It is now well established that its basic structure is the bilayer (at high q vectors, the scattering profile is the form factor of a randomly oriented bilayer) that is randomly connected and separates space into two continuous equivalent subvolumes. As put into evidence by the broad maximum at q_0, visible in the scattering profile, the sponge phase has no long-range order in opposition with lamellar and cubic phases, but it keeps a correlation distance $\xi = 2\pi/q_0$ that corresponds to the mean distance between the bilayers.

In our system, the sponge phase locates near the cubic phase and extends from 38 to 60 wt % of surfactant and from 5 to 25 °C. There is also a wide biphasic region where it coexists with the lamellar phase. Figure 8 displays the correlation distance ξ and the dry bilayer thickness δ as a function of the water amount represented by α. The characteristic distance is directly related to the surfactant volume fraction Φ^S:

$$\xi = \frac{k\delta}{\Phi^S_V} \tag{7}$$

where k is a geometrical parameter whose value has been estimated to be 1.25.[16] From Figure 8, we deduce that $\delta = 31 \pm 1$ Å. In the lamellar phase the plot d versus the inverse of the surfactant volume fraction gives the same value ($\delta = 30 \pm 1$ Å).

7. Discussion

A comparative study of fluorinated and hydrogenated oxyethylene surfactants shows a similar phase behavior if one takes into account the hydrophobicity difference of fluorinated and hydrogenated chains.[11] The $C_6F_{13}CH_2(EO)_n$ surfactant is roughly equivalent to $C_{12}H_{25}(EO)_{n-1}$ where EO denotes an oxyethylene group.[11] The surfactant depicted in the present paper is also composed of six fluorinated carbons chain, but the CH_2 junction is replaced by $\Sigma = C_2H_4SC_2H_4$. The analysis of the critical micellar concentrations, obtained by surface tension measurements, on the surfactants set $C_mF_{2m+1}\Sigma(EO)_n$ with $n = 2-7$ showed that the Σ moiety contributes only very little to the compound hydrophobicity.[15] If one assumes that this result can be transferred to the binary phase diagram behavior, then our surfactant should be compared to the hydrogenated $C_{12}H_{25}(EO)_2$ one. Indeed, the phase diagram of this surfactant published by Tiddy et al. exhibits the same phase sequence and the temperature range, at which the phases exist, is similar.[13]

The phase diagram reported here exhibits the classical phases usually present with hydrophobic nonionic surfactants: reverse micellar, lamellar, cubic, and sponge phases. The lamellar phase melts into two cubic phases when the temperature increases. This is characteristic of nonionic fluorinated and hydrogenated surfactants with a small polar headgroup ($C_{12}EO_2$,[4,13] $C_{16}EO_4$[30]). Indeed, as the surfactant is more hydrophilic, (i.e., $n > 3$ for the series $C_6F_{13}CH_2(EO)_n$ and $n > 2$ for the $R^F_6\Sigma EO_n$ series), no cubic phase is formed.[10,11] However, in our system, the reverse micellar phase gives rise upon dilution to a cubic phase and then to a sponge phase. This is not the case for the $C_{12}EO_2$ surfactant since there exists a transition L_2-L_3 at 30 °C. At this temperature, the cubic phase is already molten. Moreover, the lamellar phase of the $C_{12}EO_2$−water system can coexist with water whereas the lamellar phase with $R^F_6\Sigma EO_2$ coexists with the sponge phase in the dilute domain. Furthermore, our fluorinated surfactant exhibits a larger temperature and composition stable cubic and sponge domains than its hydrogenated analogue. Such a surfactant gives rise to easier experimental investigations.

As for the two cubic phases, one can remark that the *Pn*3*m* structure is much less stable against temperature and concentration than the *Ia*3*d* one and that its existence domain is situated at the cubic region border. This leads to the fact that the *Pn*3*m* structure can coexist with water, whereas the *Ia*3*d* never can. In his review on the inverse bicontinuous cubic phases, Templer drew the same conclusion: only the *Pn*3*m* and *Im*3*m* structures have been observed in excess of water.[31]

The transition between the two cubic phases can be described as a Bonnet transformation from the G surface into the D surface.[32] This transformation occurs without tearing or stretching the surface but only by bending it. Hence the lattice parameters of the two cubic structures are in the ratio 1.57.[32] By comparing them at each concentration where both structures exist, one finds a ratio close to 1.6, which is in good agreement with the theoretical value. Another way of visualizing the transformation between the two cubic structures is to seek possible epitaxial relationships. They are easily put into evidence by plotting d_{hkl} versus $(h^2 + k^2 + l^2)^{-1/2}$ for two samples of the same composition (72% in weight of surfactant) and belonging each to one of the two structures (Figure 9). On this figure the data related to the lamellar phase are added. The lattice

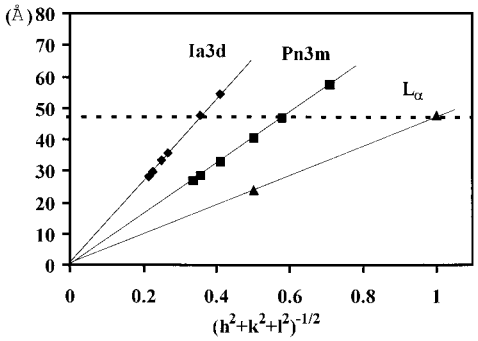

Figure 9. Repetition distance versus $(h^2 + k^2 + l^2)^{-1/2}$ in the lamellar phase (▲) and in the *Ia*3*d* (◆) and *Pn*3*m* (■) cubic phases.

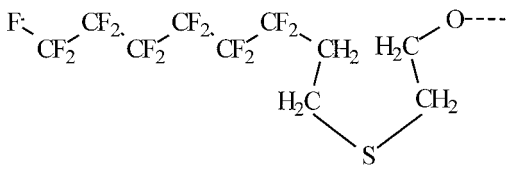

Figure 10. Proposed conformation of the surfactant hydrophobic part throughout the liquid crystal domain.

parameters are directly deduced from the slopes of these lines. The dotted line shows that $d_{100}(L_\alpha) \approx d_{220}(Ia3d) \approx d_{111}(Pn3m)$. This gives the same epitaxial relationship already observed by Funari.[4] The authors concluded that they represent the more dense planes. When the temperature increases, the lamellar planes transform into the [220] planes of the *Ia*3*d* structure and then into the [111] planes of the *Pn*3*m* structure. Other possible epitaxial relationships between the two cubic phases are given by $d_{211}(Pn3m) \approx d_{400}(Ia3d)$ and $d_{220}(Pn3m) \approx d_{322}(Ia3d)$.

Concerning the structural parameters the area per polar head S has been determined in the liquid crystal domains. In both cubic phases and in the lamellar phase, S is independent of concentration and hardly varies with temperature (less than 3% throughout the phase diagram). The surface per polar head stays almost unchanged from one phase to another, $S = 39 \pm 2$ Å^2. This result has already been encountered for several hydrogenated systems.[33,34] As the area per polar group is constant, the hydrophobic chain conformation is unchanged as well. Two ways lead to the same type of conformation. On one hand, we deduce the lengths of the chains $l_{C_6F_{13}} = 7.6$ Å and the junction $l_\Sigma = 3.5$ Å from the area per polar group and from the molar volumes 174.1 and 80.6 cm^3 mol^{-1}, respectively. On the other hand, knowing that the fluorinated C−C bonds are more rigid than the hydrogenated ones and thus than the Σ moiety, one can reasonably propose a configuration of the hydrophobic part of the bilayer. The fluorinated C−C chains arrange all in a trans conformation, and the chain $C_2H_4SC_2H_4$ is folded. A probable configuration corresponding to this scheme is reported in Figure 10. The values deduced from this scheme are $l_{C_6F_{13}} = 7.8$ Å, $l_\Sigma = 3.8$ Å, and $l_B = 11.6$ Å, they agree very well with the experimental data and the calculated values.[35] Investigations on the set of surfactants $C_6F_{13}CH_2(EO)_n$ with $n > 3$ show that the longer the polar headgroup, the more extended conformation the hydrophobic chains adopt. These results are very consistent with the fact that our surfactant with two EO groups has a relatively extended hydrophobic chain conformation, i.e., ordered fluorinated chains. This hydrophobic conformation holds for the liquid crystal domain. As to the hydrophilic part, it is folded and composition independent in the lamellar phase. The only governing parameter on the microscopic scale is the water film thickness. When the lamellar phase swells, it increases whereas the hydration (and chains conformation) of the oxyethylene head stays unchanged. We, then, wonder what is the destabilization process of the lamellar phase. The plot of the repetition distance versus the inverse of the surfactant volume fraction is linear in the whole domain and gives a dry bilayer thickness $\delta = 31$ Å. The perfect linearity shows that the bilayers are quite rigid and the lamellar phase is not stabilized via Helfrich's undulations.[36] Hence the hypothesis of a transition from the lamellar to the sponge phase by a process of undulations and holes creation seems not to occur in the present case.

Acknowledgment. We are very grateful to Laurence Mansuy for providing us with a surfactant having a very high degree of purity. Preliminary SAXS experiments in the cubic domain were performed at Centre de Recherche Paul Pascal (Bordeaux). We would like to thank Didier Roux for his welcome and fruitful discussion and Rolf Klucker for his participation to the experiments. The study of the cubic phase would not be so precise without the use of the D43 line, so we would like to acknowledge Jean Doucet for according us time. We are also very grateful to Dominique Durand for her help during these experiments.

References and Notes

(1) Mariani, P.; Luzzati, V.; Delacroix, H. *J. Mol. Biol.* **1988**, *204*, 165. Fontell, K. *Advances Colloid Interface Sci.* **1992**, *41*, 127. Larsson, K. *Lipids-Molecular Organization Physical functions and Technical Applications*; The Oily Press: 1994; Vol. 5.

(2) Luzzati, V.; Spegt, P. A. *Nature* **1967**, *215*, 701.

(3) Luzzati, V.; Tardieu, A.; Gulik-Kryzwicki, T.; Rivas, E.; Reiss-Husson, F. *Nature* **1968**, *220*, 485.

(4) Funari, S.; Rapp, G. *J. Phys. Chem. B* **1997**, *101*, 732.

(5) Rançon, Y.; Charvolin, *J. Phys. Chem.* **1988**, *92*, 2646.

(6) Landau, E. M.; Rummel, G.; Cowan-Jacob, S. W.; Rosenbuch, J. P. *J. Phys. Chem. B* **1997**, *101*, 1935.

(7) Razumas, V.; Larsson, K.; Milzis, Y.; Nylander, T. *J. Phys. Chem.* **1996**, *100*, 11766.

(8) Engström, S. *Polymer* **1990**, *31*, 157.

(9) Ravey, J. C.; Gherbi, A.; Stébé, M. J. *Prog. Colloid Polym. Sci.* **1988**, *76*, 234.

(10) Ravey, J. C.; Stébé, M. J. *Prog. Colloid Polym. Sci.* **1987**, *73*, 127.

(11) Ravey, J. C.; Stébé, M. J. *Colloids Surf. A* **1994**, *84*, 11.

(12) Cambon, A.; Delpuech, J. J.; Matos, L.; Serratrice, G.; Szonyi, F. *Bull. Soc. Chim. Fr.* **1986**, *6*, 965.

(13) Conroy, J. P.; Hall, C.; Leng, C. A.; Rendall, K.; Tiddy, G. J. T.; Wash, J.; Lindblom, G. *Prog. Colloid Polym. Sci.* **1990**, *82*, 253.

(14) Gherbi, A.; Ait Amar, H.; Ravey, J. C. *J. Chim. Phys.* **1994**, *91*, 89.

(15) Matos, L.; Ravey, J. C.; Serratrice, G. *J. Colloid Interface Sci.* **1989**, *128*, 341.

(16) Ravey, J. C.; Stébé, M. J.; Sauvage, S.; El Moujahid, C. *Colloids Surf. A* **1995**, *99*, 221.

(17) Nallet, F.; Laversanne, R.; Roux, D. *J. Phys. II Fr.* **1993**, *3*, 487.

(18) Rösch, M. In *Non ionic Surfactants*; Schick M. J.; Eds.; Surfactant Science Series Vol. 1; Dekker: New York, 1996; p 753.

(19) Boretta, M.; Cantù, L.; Corti, M.; Del Favero, E. *Physica A* **1997**, *236*, 162.

(20) Ström, P.; Anderson, D. *Langmuir* **1992**, *8*, 691.

(21) Tiddy, G. J. T.; Rendall, K.; Galsworthy, P. *Mol. Cryst. Liq. Cryst.* **1982**, *72*, 147.

(22) Clerc, M.; Hendrikx, Y.; Farago, B. *J. Phys. II Fr.* **1997**, *7*, 1205.

(23) Imai, M.; Kato, T.; Schneider, D. *J. Chem. Phys.* **1997**, *106*, 9362.

(24) Scriven, L. *Nature* **1976**, *93*, 123.

(25) Clerc, M.; Levelut, A. M.; Sadoc, J. F. *J. Phys. II Fr.* **1991**, *1*, 1263.

(26) Gulik, A.; Luzzati, V.; De Rosa, M.; Gambacorta A. *J. Mol. Biol.* **1985**, *182*, 131. There is a misprint in k_S of *Pn*3*m*: it should read 1.168 instead of 1.068.

(27) Hyde, S. T. *J. Phys. Chem.* **1989**, *93*, 1458.

(28) Cates, M. E.; Roux, D.; Andelman, D.; Milner, S. T.; Safran, S. A. *Europhys. Lett.* **1988**, *5*, 733.

(29) Porte, G.; Marignan, J.; Bassereau, P.; May, R. *J. Phys.* **1988**, *49*, 511.

(30) Mitchell, D. J.; Tiddy, G. J. T.; Waring, L.; Bostock, T.; McDonald, M. P. *J. Chem. Soc., Faraday Trans. 1* **1983**, *79*, 975.
(31) Templer, R. H. *Curr. Opin. Colloid Interface Sci*. **1998**, *3*, 255.
(32) Benedicto, A. D.; O'Brien, D. F. *Macromolecules* **1997**, *30*, 3395.
(33) Alibrahim, M.; Stébé, M. J.; Dupont, G.; Ravey, J. C. *J. Chim. Phys.* **1997**, *94*, 1614
(34) Kunieda, H.; Ozawa, K.; Huang, K. L. *J. Phys. Chem. B* **1998**, *102*, 831.
(35) We used the following lengths: C−C = 1.5 Å, C−S = 1.8 Å, C−F = 1.3 Å, and angles, CCC = CCS = 109°, CSC = 105°, and CCF = 110°.
(36) Helfrich, W. Z. *Naturforsh. A* **1978**, *33*, 305.